A bithiophene-substituted porphyrin displaying multi-electron redox processes as a cathode for lithium organic batteries

Shagor Chowdhury[a,b]*, Saibal Jana[a], Svetlana Klayatskaya[a]* and Mario Ruben[a,b,c]*

[a]*Institute of Nanotechnology (INT), Karlsruhe Institute of Technology (KIT), Eggenstein-Leopoldshafen D-76344, Germany*

[b]*Centre Européen de Sciences Quantiques (CESQ), Institut de Science et d'Ingénierie Supramoléculaires (ISIS), Strasbourg Cedex F-67083, France*

[c]*Institute for Quantum Materials and Technology (IQMT), Karlsruhe Institute of Technology (KIT), Eggenstein Leopoldshafen D-76344, Germany*

ABSTRACT: A non-metallated porphyrin, 5,15-di([2,2′-bithiophen]-5-yl)-10,20-diphenylporphyrin (**BTPP**) has been synthesized and utilized as an electrode material for lithium organic batteries (LOBs). Benefiting from the bipolar characteristics of the porphyrin core and extended π-conjugation with bithiophene units, **BTPP** displayed as cathode material a discharge capacity of 128 mAh. g^{-1} at a current density of 0.2 A. g^{-1}, with an average discharge voltage of 3.2 V and showed a good rate capability. At a high current density of 10 A. g^{-1}, it delivered a discharge capacity of 32 mAh. g^{-1}.

KEYWORDS: Porphyrin, Lithium organic cathode, Energy storage system

INTRODUCTION

Lithium-ion batteries (LIBs) have emerged as the primary energy source for versatile portable devices (smartphones, laptops, electronic watches) and electric vehicles (EVs) [1]. However, their increasing demand has created significant challenges in utilizing lithium-based transition metal oxides and phosphates in conventional lithium-ion batteries. The main hurdle relies on the manufacturing process of the conventional inorganic electrode material that requires plenty of resources and generates environmentally detrimental waste products [2–3].

Organic electrode materials have been considered the most promising candidates for next-generation lithium-organic batteries. The main advantages of using organic compounds rely on their lower CO_2 footprint, abundant reserves and precisely controllable synthesis with excellent electrochemical properties [4–5]. However, they usually suffer from a major limitation, which is their tendency to dissolve in electrolytes and low conductivity [6]. Several approaches have been implemented to address the aforementioned issues which include the chemical and electrochemical polymerization of the material beforehand [7–10], or *in-situ* electrochemical polymerization of the material during the cycling process [11–12]. Another strategy relies on expanding the π-conjugated system through the introduction of functional conjugated units [13–14]. For instance, studies on benzoquinone [15], anthraquinone [16], and pentacene tetraone [17–18] have demonstrated that enhancement in cycling stability can be achieved by reducing solubility through the expansion of π-conjugation.

Porphyrins are highly conjugated flat macrocyclic structures that are well-known for their wide range of applications in oxygen transportation, catalysis and light harvesting [19–21], and they have recently emerged as a promising class of organic electrode materials due to their fast redox kinetics and bipolar properties [22–29]. Its bipolar properties enable it to possess the characteristics of both n-type and p-type materials and during the

*Correspondence to: Shagor Chowdhury, email: schowdhury@unistra.fr, Svetlana Klyatskaya, e-mail: svetlana.klyatskaya@kit.edu, Mario Ruben, e-mail: mario.ruben@kit.edu.

redox processes the charges are stabilized in the mesomeric core via fast electron release and uptake [12, 30]. Recently, it has been shown that the performance of porphyrin-based electrode materials is usually dictated by their planarity, efficient packing, crystallinity and solubility [31]. Moreover, tetraphenyl porphyrins have shown poor performance in lithium-ion batteries because of their high solubility in the electrolyte [26]. To mitigate the undesired solubility, the introduction of different conjugated substituents can be an effective approach to improve structural stability. Based on theoretical studies (Fig. S1), it was found that porphyrin with bithiophene would reduce the highest and lowest molecular orbital energy gap thus rendering it with improved electronic conductivity and thus facilitating the charge transfer which will be beneficial to improve the cycling stability and the rate capability of the material [32–34]. Therefore, bithiophene substituted porphyrin 5,15-di([2,2′-bithiophen]-5-yl)-10,20-diphenylporphyrin (**BTPP**) was synthesized and its electrochemical properties were studied in view of its potential application as electrodes in LIBs.

RESULTS AND DISCUSSION

Synthesis

The multi-step synthesis of the desired bithiophene functionalized porphyrin (**BTPP**) is outlined in Scheme 1. The intermediate ABAB meso-free porphyrin (**1**) was prepared using a previously established method [35]. It involved the Brønsted acid-catalyzed condensation of 2,2′-dipyrrolylmethane with the benzaldehyde followed by oxidation with DDQ. Then the key intermediate **2** was obtained by regioselective bromination of the two meso-free positions with N-bromosuccinimide. Subsequently, the Suzuki-Miyaura cross-coupling reaction between intermediate **2** and 2,2′−Bithiophene-5-boronic acid pinacol ester afforded **BTPP** in 45% yield. The successful synthesis of **BTPP** was confirmed by ^{1}H-NMR spectroscopy and fully characterized using 1D- and 2D-NMR experiments. Detailed attribution of the aromatic ^{1}H signals is shown in Fig. S8. The high-resolution mass spectrometry has further supported the formation of **BTPP** by the presence of the peak at m/z = 791 (Fig. S9). The absorption spectrum of **BTPP** recorded in dichloromethane exhibited one intense Soret band centered at λ_{max} = 426 nm (ε = 292600 mol.l^{-1}.cm^{-1}) and four much weaker Q bands (Fig. S10). The PXRD pattern of **BTPP** indicated the crystalline nature of the molecule (Fig. S11). For morphological characterization, scanning electron microscopy (SEM) was employed and it displayed **BTPP** in the form of a two-dimensional crystalline structure (Fig. S12).

Electrochemical characterization of BTPP

The ability of the porphyrins to undergo multiple electron transfers through oxidation (from 18π e$^-$ to 16π e$^-$) or reduction processes (from 18π e$^-$ to 20π e$^-$) has been previously illustrated through numerous investigations [20–24]. Hence these compounds could serve as an active material in energy storage systems (EESs) [8, 31]. Therefore the redox property of **BTPP** was been initially assessed using a three-electrode configuration cyclic voltammetry (CV) in dichloromethane using tetra-n-butylammonium hexafluorophosphate ($TBAPF_6$) as an electrolyte (Fig. 1a).

The CV curves displayed two successive reduction and two successive oxidation waves centered on the porphyrin ring within the accessible potential window. At the cathodic side, the reduction waves centered at $E_{1/2}$ = -1.15 V and -1.52 V are attributed to the one-electron reduction of **BTPP** into the radical anion (**BTPP$^{\bullet-}$**) and the reduction of (**BTPP$^{\bullet-}$**) into the dianionic species (**BTPP^{2-}**), respectively. Whereas at the anodic side, the oxidation waves centered at $E_{1/2}$ = 0.94 V and 1.05 V are attributed to one-electron oxidation of **BTPP** into the radical cation (**BTPP$^{\bullet+}$**) and oxidation of (**BTPP$^{\bullet+}$**) into the dicationic (**BTPP^{2+}**), respectively. It is worth mentioning that the electrochemical activity of the bithiophene unit has not been observed within the selected voltage window, most probably due to its high stability that may require higher potential to be accessed or require the use of different working electrode like ITO as shown by Wu and coworkers [36–37]. Further insights into the attribution of these electron transfers have been obtained from the spectroelectrochemical (SEC) experiments.

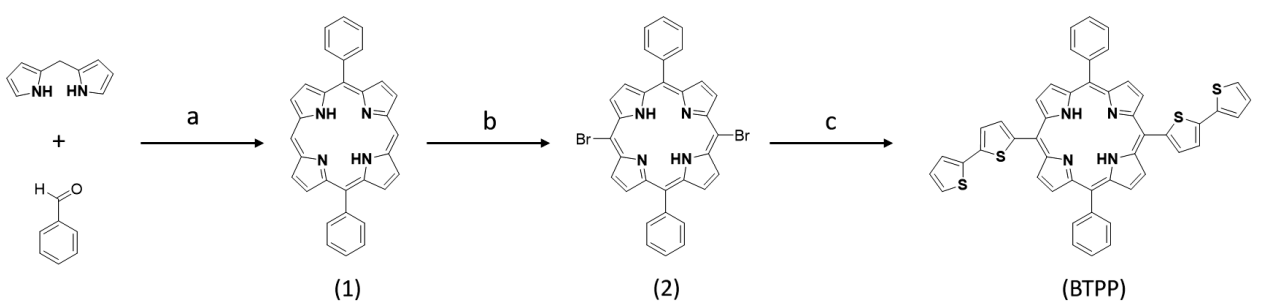

Scheme 1. Synthetic route of BTPP. (a) CH_2Cl_2, TFA, DDQ , 28 °C, 4 h, 72 %. (b) CH_2Cl_2/MeOH, NBS, 0 °C, 1 h, 80 %. (c) $Pd(PPh_3)_4$, 2,2′−Bithiophene-5-boronic acid pinacol ester, K_2CO_3, DMF, 110 °C, 48 h, 45 %.

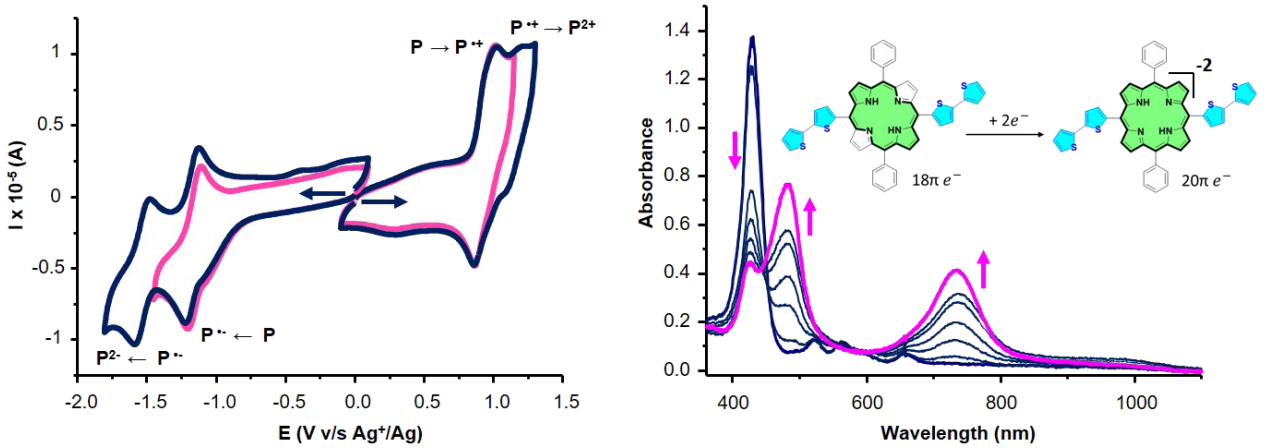

(a) (b)

Fig. 1. (a) CV of BTPP (1 mM) in a 0.1 M $TBAPF_6/CH_2Cl_2$ supporting electrolyte/solvent at a scan rate of 100 mV. s^{-1}. (b) UV–vis spectra recorded during two-electron reduction of BTPP in CH_2Cl_2 containing 0.1 M $TBAPF_6$ (working electrode: Pt, l = 1 mm).

Those measurements were carried out upon collecting time-resolved UV–vis spectra during the electrochemical reduction/oxidation of **BTPP** using a platinum gauze electrode in a thin-layer SEC cell with a 1 mm thickness. The SEC data collected upon scanning the working electrode potential from 0 to -1.90 V resulted in the gradual decrease in the intensity of the initial Soret band located at 426 nm at the expense of less intense signals developing at λ_{max} = 482 (Fig. 1b). The presence of an isosbestic point at 444 nm further confirms that no secondary reactions occur over the considered time range. The Q bands were also found to disappear at the expense of new bands developing at λ_{max} = 734 nm. A similar analysis has been performed by scanning the working electrode potential from 0 to 1.50 V and it led to the increase in the intensity of the Soret band and Q band with the appearance of new bands centered at λ_{max} = 483, 745 and 982 nm. Then, the Soret band lost ¾ of its intensity and the Q bands disappeared, while the intensities of the bands centered at λ_{max} = 483, 745 and 982 nm increased (Fig. S13). These findings are consistent with the formation of the anionic and cationic porphyrin species upon reduction and oxidation, respectively and that the observed electron transfers involve the porphyrin macrocycle [38–40].

Charge storage property of BTPP as cathode

The charge storage properties of **BTPP** as a cathode material were tested within the voltage range of 1.80 – 4.50 V in a half-cell using lithium as an anode and $LiPF_6$ (1 M in ethylene carbonate : dimethyl carbonate) as electrolyte using cyclic voltammetry (CV) at a scan rate of 0.1 mV. s^{-1} (Fig. 2a). During the initial anodic scan, strong irreversible oxidation peaks appeared at 4.07 V and 4.19 V, which is attributed to the oxidation of **BTPP** into cationic species **[BTPP]$^{2+}$**. The occurrence of an irreversible process at higher potential is a typical characteristic of porphyrin-based compounds and it results from the formation of the cathode electrolyte interface and the distortion of the structure upon the interaction with PF_6^- ions (Fig. S14) [9, 41–43]. Whereas in the reverse cathodic scan, four peaks were detected at 4.15 V, 3.79 V, 2.66 V, and 2.50 V. These peaks are associated with the one-electron reduction processes of **[BTPP]$^{2+}$** into **[BTPP]$^{2-}$**. In the second cycle, four oxidation and four reduction peaks were recorded, where the oxidation peaks at 2.58 V and 3.32 V represent the oxidation of **[BTPP]$^{2-}$** into **BTPP** and the peaks at 3.89 V and 4.18 V represent the oxidation of **BTPP** into **[BTPP]$^{2+}$**. Afterward, the CV curves were well overlapped, suggesting the high reversibility and cycling stability of the **BTPP** electrode. To our knowledge, it is one of the few cases in which the four-electron transfers centered on the porphyrin in lithium-based half cells are recognizable over repeated cycles within the selected voltage range [12, 26, 44–47].

Galvanostatic charge/discharge profiles were recorded at a current density of 0.2 A. g^{-1} and they displayed a consistent outcome with the CV data (Fig. 2b). During the first cycle, irreversible charge/discharge capacities (152/129 mAh. g^{-1}) were observed. In the following, highly reversible processes were found with the appearance of charge/discharge voltage plateaus that are closely aligned with the peaks observed in the CV curves, indicating the presence of a multi-electron transfer mechanism with similar reaction pathways throughout the cycling [48]. Such stable voltage plateau over repetitive cycles is relatively rare for porphyrin-based electrode materials that might be a result of the extended π-conjugation [34, 49]. During the second cycle a discharge capacity of 128 mAh. g^{-1} was delivered with an average discharge voltage of 3.2 V and a specific energy density of 412 Wh. Kg^{-1}. Moreover, the discharge capacity recorded was close to the theoretical value of 135 mAh. g^{-1} associated to the four-electron reactions (**[BTPP]$^{2+}$** → **[BTPP]$^{2-}$**).

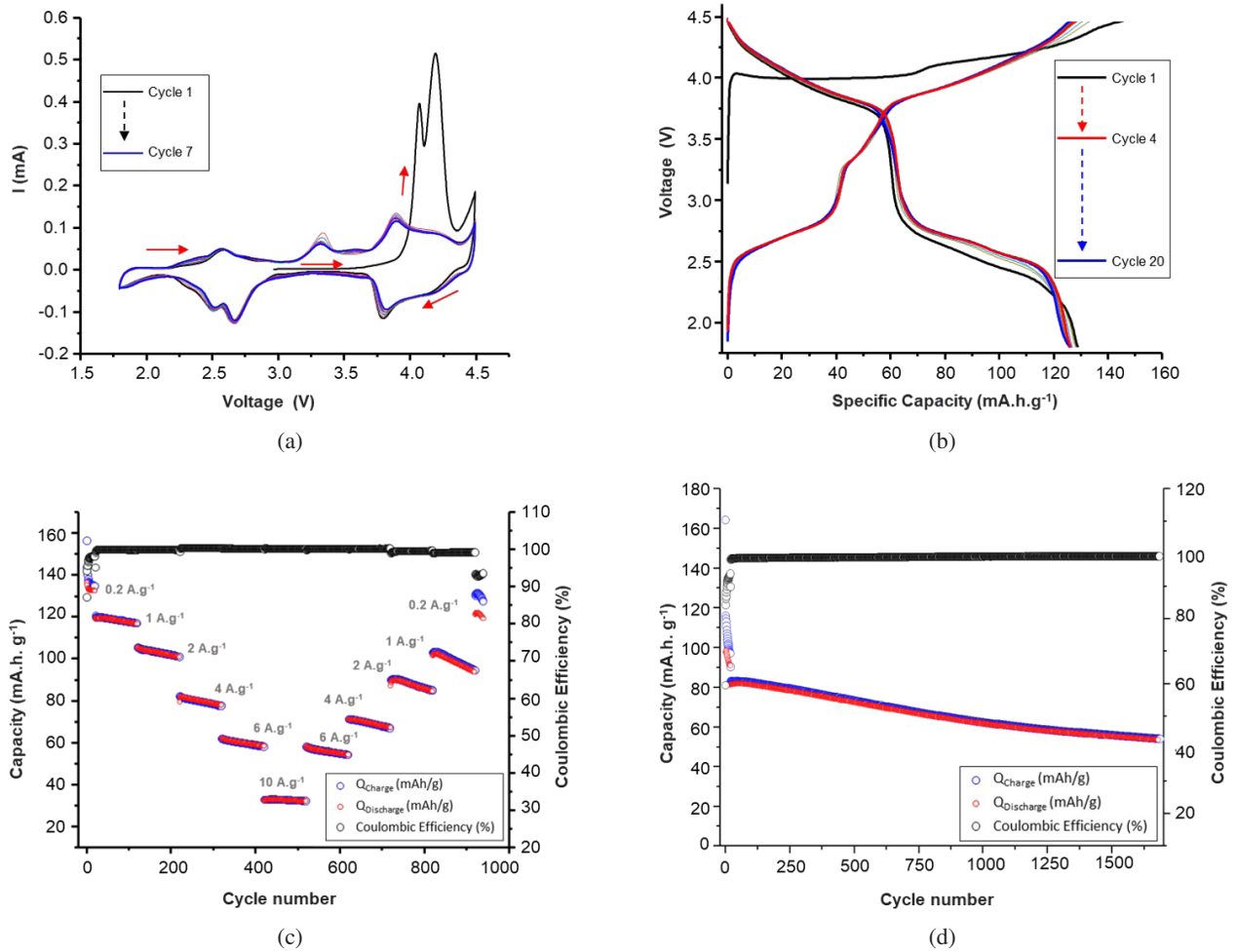

Fig. 2. (a) Selected CVs in the range of 4.5–1.8 V at a scan rate of 0.1 mV. s^{-1}. (b) Charge and discharge profiles at 200 mA. g^{-1}. (c) Representation of the rate capability of BTPP. (d) Cycling performance of BTPP cathode.

Herein, the capacity contribution from carbon black is negligible (Fig. S15). The rate performance of the electrode was then assessed at various current densities from 0.2 to 10 A. g^{-1}. The cell was initially charged/discharged at 0.2 A. g^{-1} (1.5C) for 20 cycles and then cycled at elevated current densities for 100 cycles at each rate (Fig. 2c). The capacity decreased upon increasing the current density. Herein, the electrode delivered reversible capacities of 118, 103, 80, 60 and 32 mAh. g^{-1} at 1 A. g^{-1} (7C), 2 A. g^{-1} (14C), 4 A. g^{-1} (29C), 6 A. g^{-1} (44C) and 10 A. g^{-1} (74C), respectively with a coulombic efficiency close to 100 %. Interestingly, when the current density was switched back to 0.2 A. g^{-1}, the recovered capacity was 121 mAh. g^{-1} which demonstrates a good rate capability of the material. The long-term cycling stability of the **BTPP** cathode was further tested at 1 A. g^{-1} after it was initially operated at 0.2 A. g^{-1} for 20 cycles (Fig. 2d). The electrode displayed good cyclic stability, where after 1700 cycles 64% of the original capacity was retained (cycle 21 to cycle 1700). Further insights into the electrochemical properties of **BTPP** were obtained by electrochemical impedance spectroscopy (EIS) (Fig. S16). The high-frequency region reveals that the charge-transfer resistance of the **BTPP** electrode was significantly reduced after the initial cycle, suggesting the enhancement of the electrical conductivity of the material.

Electrostatic potential (ESP) distributions have been used to investigate the interaction sites between the active material (**BTPP**) and the anions/cations (Li^+/PF_{6^-}) (Fig. S17) [50]. In line with previously investigated porphyrin-based electrode material [9, 26, 51], the area near the N atoms of the porphyrin ring in **BTPP** displayed high affinity toward PF_{6^-} and Li^+ ions in both charged and discharged states, respectively.

CONCLUSION

In summary, a bithiophene-functionalized metal-free porphyrin (**BTPP**) has been synthesized. Its bipolar reactivity endows it with multiple electron transfer properties and the extended π-conjugation with bithiophene units resulted in a stable cyclic performance as a cathode material with a discharge capacity of 128 mAh.g^{-1} at 0.2 A. g^{-1} and a good rate capability. At a high current density of

10 A. g^{-1}, the electrode delivered a reversible charge/discharge capacity of 32 mAh. g^{-1}. Therefore, **BTPP** is a promising high-rate organic cathode material for lithium batteries. This work provides new insights toward the development of organic compounds for electrochemical energy storage devices.

EXPERIMENTAL

General

All reagents were obtained commercially unless otherwise noted. All reactions were performed in oven-dried glassware (Schlenk flasks) under an argon atmosphere. All solvents were dried and distilled by standard procedures. Thin-layer chromatography was performed on aluminum plates pre-coated with Merck 5735 silica gel 60 F254. Column chromatography was performed with Merck silica gel 60 (230 – 400 mesh).

^{1}H NMR spectra were recorded on Bruker Avance 400 (400 MHz for ^{1}H) and Bruker Ascend Spectroscope Avance Neo-500 MHz (500 MHz for ^{1}H); chemical shifts are given in ppm using residual proton resonances of the solvents as references. Coupling constants values (J) are given in hertz and chemical shifts (δ) in ppm. The abbreviations used are: s = singlet, d = doublet, t = triplet, m = multiplet and br = broad. UV-VIS spectra were measured on a Varian Cary 500 Scan UV/VIS/NIR spectrophotometer. Mass spectrometry measurements were carried out using Thermofischer Ultimate3000 with Scientific Vanquish Flex UHPLC with electrospray ionization (ESI) and Maldi Autoflex speed Bruker. Scanning electron microscope (SEM) was carried out using a ZEISS LEO 1530 instrument with an X-Max Silicon Drift Detector.

Cyclic voltammetry (CV) was measured using Autolab PGSTAT100 or PGSTAT204. The typical three-electrode setup was used, with a glassy carbon electrode (diameter = 3 mm), a platinum wire electrode, and a silver wire as working electrode, counter electrode, and reference electrode, respectively. All analyses were performed in dry dichloromethane in the presence of tetrabutylammonium hexafluorophosphate ($TBAPF_6$) as a supporting electrolyte. The system was kept inside the Faraday cage to minimize electrical noise. All the measurements were carried out at room temperature (20–23 °C).

Spectroelectrochemistry experiments were performed with Autolab PGSTAT204, using the typical three-electrode setup with a platinum grid (WE), a platinum wire (CE) and a silver wire (RE). 1 mL solution was inserted in a 0.1 cm pathlength cuvette and degassed using a solvent-saturated Argon flow. All the measurements were carried out at room temperature (20–23 °C). OPTOPRIM Avantes Avalight-DHC Deuterium-hydrogen lamp was used to cover the visible-IR region, whereas Avantes Sensline Avaspect-ULS2048XL-EVO was used as a detector.

Electrode Preparation: The electrode slurry was prepared by mixing 50 wt % of porphyrin-based active materials with 40 wt % of Super P conductive carbon (role: improve conductivity), and 10 wt% of poly(vinylidene difluoride) (PVDF) (role: binder) with N-methyl pyrrolidone (NMP) as solvent. The slurry was drop casted on a stainless-steel current collector (11.8 mm dia.) and dried at 100 °C overnight. After drying, the electrode discs were transferred and stored in an Argon-filled glove box.

Cell Assembly: All the assembly experiments were performed in an argon-filled glove box using a CR2032 coin-type cell (MTI Corporation), Glass fiber filters (GF/D, Whatman) were used as separator, and 1 M lithium hexafluorophosphate ($LiPF_6$) in ethylene carbonate (EC): dimethyl carbonate (DMC) (EC : DMC = 1:1 by volume ratio) as electrolyte.

For Li-ion half cells: Lithium foil was used as a counter electrode. The potential of 1.8–4.5V (Vs. Li^+/Li). Capacities were calculated based on the active material of the electrode.

Electrochemical Cell Tests: Electrochemical cell tests of cyclic voltammetry, charge-discharge cycling and rate capability tests were performed on a Biologic VMP-3 potentiostat and a Biologic BCS 805 battery testing unit. Electrochemical impedance spectroscopy (EIS) was performed using AC frequencies between 50000 MHz and 1000 MHz. The measurement was always performed after a 1 h OCV period to minimize polarization effects.

DFT calculations were performed in the Orca 5.0.1 package [52] using the B3LYP-D3(BJ)/def2-TZVP [53–57] level of theory. This method involves hybrid functional B3LYP and triple-ζ quality basis set def2-TZVP, and third generation of Grimme's empirical dispersion correction (D3), with Becke-Johnson damping function (BJ). The converged structures were energetic minima, as established by frequency calculations.

Synthesis

***2,2′-Dipyrromethane*:** The intermediate was synthesized as described in the literature [58]. ^{1}H NMR (400 MHz, $CDCl_3$) δ 7.87 (broad s, 2H), 6.66 (d, J = 1.6 Hz, 2H), 6.23 – 6.09 (m, 2H), 6.04 (s, 2H), 3.98 (s, 2H).

***5,15-Diphenylporphyrin (1)*:** The intermediate was synthesized as described in the literature [35]. ^{1}H NMR (500 MHz, $CDCl_3$) δ 10.33 (s, 2H), 9.41 (d, J = 4.5 Hz, 4H), 9.09 (d, J = 4.5 Hz, 4H), 8.29 – 8.27 (m, 4H), 7.82 (dd, J = 4.2, 2.2 Hz, 6H), -3.11 (s, 2H).

***5,15-Dibromo-10,20-diphenylporphyrin (2)*:** The intermediate was synthesized as described in the literature [35]. ^{1}H NMR (500 MHz, $CDCl_3$) δ 9.62 (d, J = 4.7 Hz, 4H), 8.84 (d, J = 3.1 Hz, 4H), 8.23 – 8.10 (m, 4H), 7.88 – 7.68 (m, 6H), -2.72 (s, 2H).

***5,15-di([2,2′-bithiophen]-5-yl)-10,20-diphenylporphyrin (BTPP)*:** To a flame-dried flask, intermediate (2) (1 g, 1.61×10^3 mol) and 2,2′–Bithiophene-5-boronic

acid pinacol ester (1.41 g, $4.83x10^{-3}$ mol) were introduced and dissolved with DMF (100 ml). Then $Pd(PPh_3)_4$ (0.35 g, $3x10^{-4}$ mol) and K_3PO_4 (62 mg, $4.5x10^{-4}$ mol) were added. The mixture was then refluxed for 24h, then the solution was evaporated under reduced pressure and the crude material was subjected to a chromatography column on silica gel using ethyl acetate/dichloromethane 1:7 as an eluent to give **BTPP** as a purple powder (0.57 g, yield 45 %). ^{1}H NMR (500 MHz, $CDCl_3$): δ 9.19 (d, J = 4.6 Hz, 4H), 8.85 (d, J = 4.6 Hz, 4H), 8.23 – 8.18 (m, 4H), 7.86 – 7.70 (m, 8H), 7.59 (d, J = 3.5 Hz, 2H), 7.43 (dd, J = 3.5, 1.0 Hz, 2H), 7.35 (dd, J = 5.2, 1.0 Hz, 2H), 7.14 (dd, J = 5.2, 3.6 Hz, 2H), -2.67 (s, 2H). HR-MS (ESI^+): calculated for $[M]^+$ m/z = 791.1426; found 791.140. UV-Vis (CH_2Cl_2, nm): 426 (ε = 292600 $mol.l^{-1}.cm^{-1}$), 520 (ε = 13000 $mol.l^{-1}.cm^{-1}$), 562 (ε = 11400 $mol.l^{-1}.cm^{-1}$), 594 (ε = 3700 $mol.l^{-1}.cm^{-1}$) and 654,4 (ε = 3200 $mol.l^{-1}.cm^{-1}$).

Acknowledgments

This work contributes to the research performed at CELEST (Center for Electrochemical Energy Storage Ulm-Karlsruhe) and was funded by the German Research Foundation (DFG) under Project ID 390874152 (POLiS Cluster of Excellence). SC wishes to thank the Foundation Jean-Marie Lehn project "QBIRAD" for the financial funding. Open Access funding is enabled and organized by Projekt DEAL.

Data availability statement

The data that support the findings of this study are openly available in Zenodo at https://doi.org/10.5281/zenodo.10727725.

REFERENCES

1. Cao C, Liang F, Zhang W, Liu H, Liu H, Zhang H, Mao J, Zhang Y, Feng Y, Yao X, Ge M and Tang Y. *Small* 2021; **17**(43): 2102233.
2. Yan X, Fan C-Y, Yang X, Wang Y-Y, Hou B-H, Pang W-L and Wu X-L. *Materials Today Energy* 2019; **13**: 302–307.
3. Yan X, Ye H, Wu X-L, Zheng Y-P, Wan F, Liu M, Zhang X-H, Zhang J-P and Guo Y-G. *J. Mater. Chem. A* 2017; **5**(32): 16622–16629.
4. Yin X, Sarkar S, Shi S, Huang Q-A, Zhao H, Yan L, Zhao Y and Zhang J. *Advanced Functional Materials* 2020: **30**(11): 1908445.
5. Liang Y and Yao Y. *Joule* 2018; **2**(9): 1690–1706.
6. Zhao Q, Zhu Z and Chen J. *Adv. Mater.* 2017; **29**(48): 1607007.
7. Tamura K, Akutagawa N, Satoh M, Wada J and Masuda T. *Macromolecular Rapid Communications* 2008; **29**(24): 1944–1949.
8. Zhao-Karger Z, Gao P, Ebert T, Klyatskaya S, Chen Z, Ruben M and Fichtner M. *Adv. Mater.* 2019; **31**(26): 1806599.
9. Yuan J, Ren B, Feng X, Gao P, Liu E and Tan S. *Chem. Commun.* 2020; **56**(40): 5437–5440.
10. Yang H, Zhang S, Han L, Zhang Z, Xue Z, Gao J, Li Y, Huang C, Yi Y, Liu H and Li Y. *ACS Applied Materials & Interfaces* 2016; **8**(8): 5366–5375.
11. Wang H-g, Wang H, Si Z, Li Q, Wu Q, Shao Q, Wu L, Liu Y, Wang Y, Song S and Zhang H. *Angew. Chem. Int. Ed.* 2019; **58**(30): 10204–10208.
12. Smok T, Abouzari-Lotf E, Frentzen S, Diemant T and Fichtner M. *Batteries & Supercaps* 2023; **6**(4): e202300026.
13. Wu H, Zhang J, Du X, Zhang M, Yang J, Zhang J, Luo T, Liu H, Xu H and Cui G. *Chem. Commun.* 2019; **55**(76): 11370–11373.
14. Kim J, Kim Y, Yoo J, Kwon G, Ko Y and Kang K. *Nature Reviews Materials* 2023; **8**(1): 54–70.
15. Hanyu Y, Ganbe Y and Honma I. *Journal of Power Sources* 2013; **221**: 186–190.
16. Lee M, Hong J, Kim H, Lim H-D, Cho S, B, Kang K and Park C, B. *Adv. Mater.* 2014; **26**(16): 2558–2565.
17. Wang C, Jiang C, Xu Y, Liang L, Zhou M, Jiang J, Singh S, Zhao H, Schober A and Lei Y. *Adv. Mater.* 2016; **28**(41): 9182–9187.
18. Ma T, Zhao Q, Wang J, Pan Z and Chen J. *Angew. Chem. Int. Ed.* 2016; **55**(22): 6428–6432.
19. Gao W-Y, Chrzanowski M and Ma S. *Chem. Soc. Rev.* 2014; **43**(16): 5841–5866.
20. Chowdhury S, Hennequin P, Cala O, Denis-Quanquin S, Saint-Aman É, Frath D, Chevallier F and Bucher C. *J. Porphyrins Phthalocyanines* 2023; **27**(07–10): 1475–1488.
21. Chowdhury S, Nassar Y, Guy L, Frath D, Chevallier F, Dumont E, Ramos AP, Demets G, J-F and Bucher C. *Electrochim. Acta* 2019; **316**: 79–92.
22. Kakui T, Sugawara S, Hirata Y, Kojima S and Yamamoto Y. *Chem. Eur. J* 2011; **17**(28): 7768–7771.
23. Liu C, Shen D-M and Chen Q-Y. *J. Am. Chem. Soc.* 2007; **129**(18): 5814–5815.
24. Yamamoto Y, Yamamoto A, Furuta S-y, Horie M, Kodama M, Sato W, Akiba K-y, Tsuzuki S, Uchimaru T, Hashizume D and Iwasaki F. *J. Am. Chem. Soc.* 2005; **127**(42): 14540–14541.
25. Liao M-S and Scheiner S. *The Journal of Chemical Physics* 2002; **117**(1): 205–219.
26. Gao P, Chen Z, Zhao-Karger Z, Mueller JE, Jung C, Klyatskaya S, Diemant T, Fuhr O, Jacob T, Behm RJ, Ruben M and Fichtner M. *Angew. Chem. Int. Ed.* 2017; **56**(35): 10341–10346.

27. Philipp T, Neusser G, Abouzari-Lotf E, Shakouri S, Wilke FDH, Fichtner M, Ruben M, Mundszinger M, Biskupek J, Kaiser U, Scheitenberger P, Lindén M and Kranz C. *Journal of Power Sources* 2022; **522**: 231002.
28. Lin X-M, Wu D-Y, Gao P, Chen Z, Ruben M and Fichtner M. *Chem. Mater.* 2019; **31**(9): 3239–3247.
29. Chowdhury S, Sabi N, Cordoba Rojano R, Le Breton N, Boudalis AK, Klayatskaya S, Dsoke S and Ruben M. *Batteries & Supercaps* 2024; e202300285.
30. Xie M, Liu J, Dai L, Peng H and Xie Y. *RSC Adv.* 2023; **13**(35): 24699–24730.
31. Shakouri S, Abouzari-Lotf E, Chen J, Diemant T, Klyatskaya S, Pammer FD, Mizuno A, Fichtner M and Ruben M. *ChemSusChem* 2023; **16**(3): e202202090.
32. Zhang M, Zhou W and Huang W. *Journal of Energy Chemistry* 2021; **57**: 291–303.
33. Shimizu A, Ishizaki Y, Horiuchi S, Hirose T, Matsuda K, Sato H and Yoshida J-i. *J. Org. Chem.* 2021; **86**(1): 770–781.
34. Peng H, Xiao J, Wu Z, Zhang L, Geng Y, Xin W, Li J, Yan Z, Zhang K and Zhu Z. *CCS Chemistry* 2022; **5**(8): 1789–1801.
35. Jiang X, Gou F and Jing H. *Journal of Catalysis* 2014; **313**: 159–167.
36. Muraoka H, Ozawa K and Ogawa S. *Heteroatom Chemistry* 2018; **29**(5–6): e21455.
37. Wu X, Zhou W, Ye C, Zhang J, Liu Z, Yang C, Peng J, Liu J and Gao P. *Angew. Chem. Int. Ed.* 2024; e202317135.
38. Ke X, Kumar R, Sankar M and Kadish KM. *Inorg. Chem* 2018; **57**(3): 1490–1503.
39. Pascal S, Bucher L, Desbois N, Bucher C, Andraud C and Gros CP. *Chem. Eur. J* 2016; **22**(14): 4971–4979.
40. Grover N, Sankar M, Song Y and Kadish KM. *Inorg. Chem* 2016; **55**(2): 584–597.
41. Gong L, Yang X, Gao Y, Yang G, Yu Z, Fu X, Wang Y, Qi D, Bian Y, Wang K and Jiang J. *J. Mater. Chem. A* 2022; **10**(31): 16595–16601.
42. Otteny F, Perner V, Wassy D, Kolek M, Bieker P, Winter M and Esser B. *ACS Sustainable Chemistry & Engineering* 2020; **8**(1): 238–247.
43. Chowdhury S, Jana S, Panguluri SPK, Wenzel W, Klayatskaya S and Ruben M. *ChemSusChem* 2024; e202301903.
44. Zeng Y, Zhou J, Zhang J, Liao Y, Sun C, Su Y, Gao P and Tan S. *Chem. Commun.* 2023; **59**(33): 4962–4965.
45. Zhang J, Ye C, He F, Zeng Y, Xiao J, Yang X, Shu H, Qi H, Liu W and Gao P. *ChemSusChem* 2023; **16**(7): e202202159.
46. Sun Y, He F, Huang X, Ren B, Peng J, Chen D, Hu X, Sun X and Gao P. *Chemical Engineering Journal* 2023; **451**: 138734.
47. Feng X, Wu X, Chen X, Yuan J, Lv S, Ren B, Sun X, Liu E, Tan S and Gao P. *Energy Storage Materials* 2021; **42**: 454–463.
48. Zhang H, Zhang R, Liu X, Ding F, Shi C, Zhou Z and Zhao N. *J. Mater. Chem. A* 2021; **9**(44): 24915–24921.
49. Tang M, Zhu S, Liu Z, Jiang C, Wu Y, Li H, Wang B, Wang E, Ma J and Wang C. *Chem* 2018; **4**(11): 2600–2614.
50. Lu Y, Hou X, Miao L, Li L, Shi R, Liu L and Chen J. *Angew. Chem. Int. Ed.* 2019; **58**(21): 7020–7024.
51. He F, Zhou Y, Chen X, Wang T, Zeng Y, Zhang J, Chen Z, Liu W and Gao P. *Chem. Commun.* 2023; **59**(19): 2787–2790.
52. Neese F. *WIREs Computational Molecular Science* 2022; **12**(5): e1606.
53. Becke AD. *The Journal of Chemical Physics* 1993; **98**(7): 5648–5652.
54. Stephens PJ, Devlin FJ, Chabalowski CF and Frisch MJ. *J. Phys. Chem.* 1994; **98**(45): 11623–11627.
55. Grimme S, Antony J, Ehrlich S and Krieg H. *The Journal of Chemical Physics* 2010; **132**(15): 154104.
56. Grimme S, Ehrlich S and Goerigk L. *Journal of Computational Chemistry* 2011; **32**(7): 1456–1465.
57. Weigend F and Ahlrichs R. *Phys. Chem. Chem. Phys.* 2005; **7**(18): 3297–3305.
58. Littler BJ, Miller MA, Hung C-H, Wagner RW, O'Shea DF, Boyle PD and Lindsey JS. *J. Org. Chem.* 1999; **64**(4): 1391–1396.